

# The New Horizons Instrument Suite

*Glen H. Fountain, Harold A. Weaver, Dennis C. Reuter, S. Alan Stern, Ivan R. Linscott, David J. McComas, Matthew E. Hill, and Mihály Horányi*

## ABSTRACT

*The New Horizons science payload consists of seven instruments—three optical instruments, two plasma instruments, a dust sensor, and a radio science receiver/radiometer. These instruments were designed to withstand the cold conditions and low light levels in the Kuiper Belt so they could investigate the global geology, surface composition and temperature, and the atmospheric pressure, temperature, and escape rate of Pluto and its moons. The same payload was used to explore Arrokoth, the most distant object ever targeted for a flyby. The instrument suite is highly power efficient and represents a degree of miniaturization that is unprecedented in planetary exploration. This article describes the instruments and how they met challenging mission requirements with resounding success, making groundbreaking measurements and returning data that continues to shed light on the mysterious planets and smaller bodies of the outer solar system.*

## INTRODUCTION

The New Horizons instrument suite met a number of challenges to make essential contributions to the success of the mission. The instruments first had to be capable of collecting the data required to meet the mission's scientific goals, outlined in the articles by Stern and Krimigis and by Weaver et al., both in this issue. The large heliocentric distances required a high launch  $C_3$  (characteristic energy twice the excess specific energy in escape orbit) and solar arrays were nonviable for a mission going so far from the Sun, so the instruments had to meet stringent mass and power requirements to accomplish these scientific objectives. The overall mission design limited the power for the entire instrument suite to 30 W, and the mission was limited to a single radioisotope thermoelectric generator that produced 202 W

of power at Pluto (at 33 astronomical units, or au, from the Sun) in July 2015 and 190 W at the Arrokoth (provisional designation 2014 MU69) flyby (at 43 au from the Sun) in 2019. The total instrument suite mass was only ~30 kg—about half the mass of the Cassini mission imager alone. And these instruments had to meet their mission specifications after a flight of 9.5 years (to Pluto).<sup>1</sup> The New Horizons instrument suite met all three of these challenging requirements with flying colors, as described in this issue.

The New Horizons payload comprises seven instruments:

1. Ralph, itself consisting of two components: the Multispectral Visible Imaging Camera (MVIC), a visible-light imager with four color filters operating

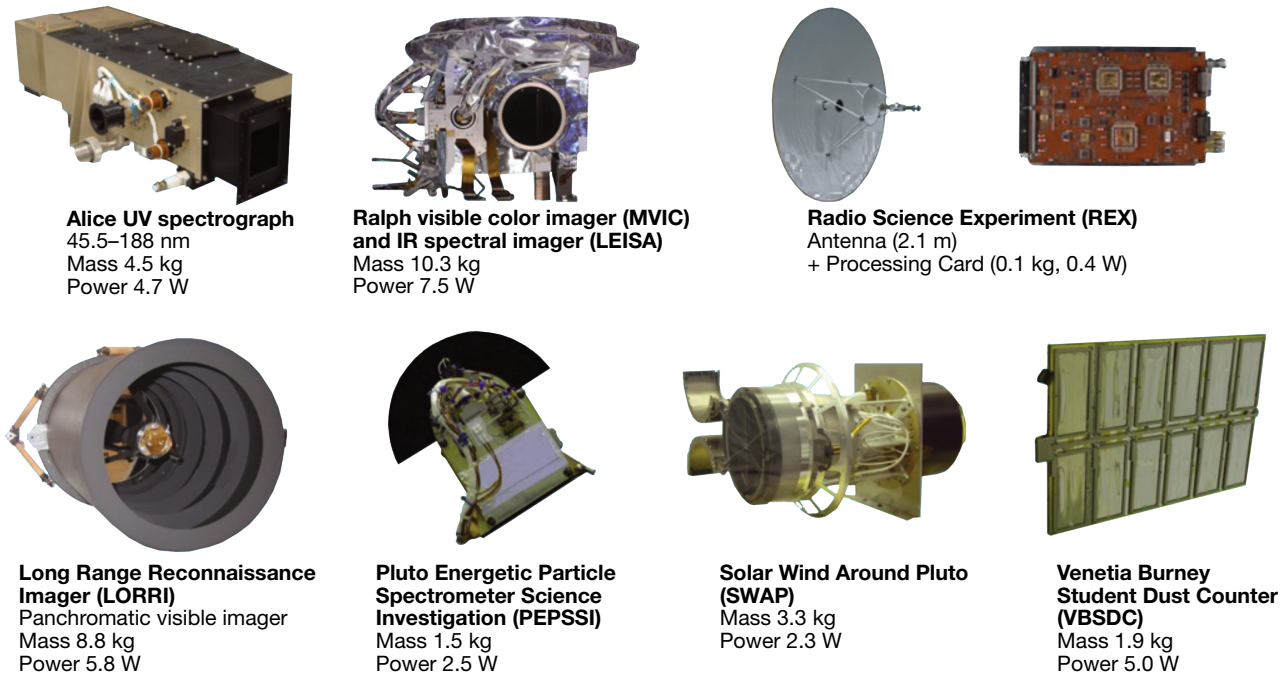


**Figure 1.** The seven instruments that make up the New Horizons payload. Approximate values for mass and power consumption are shown just below the picture of each instrument. The total mass of the entire science payload is ~30 kg, excluding the antenna, and the total power drawn by all the instruments is ~28 W. The entrance apertures of the remote sensing instruments are 4.0 cm, 7.5 cm, 20.8 cm, and 2.1 m across for Alice (airglow channel), Ralph, LORRI, and the REX high-gain antenna (HGA), respectively. The SWAP and PEPSSI apertures are ~20 cm across. Each of the 12 polyvinylidene chloride (PVDC) panels in the VSDC are 14.2 cm × 6.5 cm. (Adapted from Weaver et al. 2008.<sup>2</sup>)

in time delay integration (TDI) mode and with panchromatic imaging in both TDI and frame-transfer mode; and the Linear Etalon Imaging Spectral Array (LEISA), a near-infrared (near-IR) spectral imager used for compositional mapping

- Alice, an ultraviolet (UV) imaging spectrograph that investigates atmospheres via solar and stellar occultations and airglow measurements
- Radio Science Experiment (REX), used for atmospheric occultation studies and radiometry
- Long Range Reconnaissance Imager (LORRI), a panchromatic visible-light imager providing high spatial resolution and high sensitivity, in addition to optical navigation
- Solar Wind Around Pluto (SWAP), a low-energy plasma instrument that measures the density and speed of solar wind particles
- Pluto Energetic Particle Spectrometer Science Investigation (PEPSSI), a high-energy plasma instrument that measures pickup ions (PIs)
- Venetia Burney Student Dust Counter (VSDC), an instrument designed and built by students to measure dust particle impacts along the spacecraft trajectory

Photos of the instruments are shown in Figure 1, and their arrangement on the spacecraft is illustrated in Figure 2. Technical details and the specific scientific objectives for each instrument are provided in Table 1. The pages that follow summarize each instrument's design and performance.

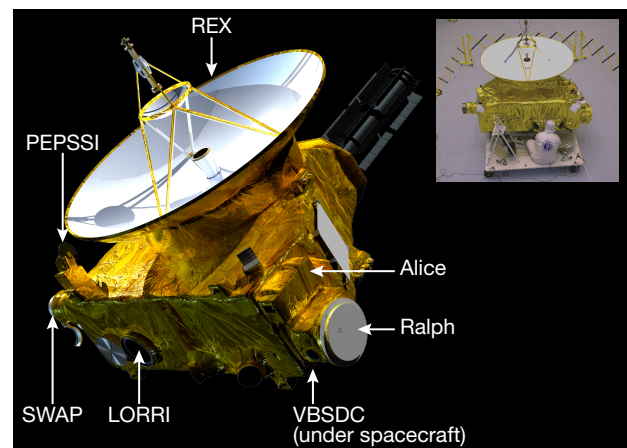


**Figure 2.** The New Horizons spacecraft with instrument layout. The photo in the upper right provides a sense of scale of the spacecraft and instruments. Additional information on the positioning and orientation of the instruments is provided in the article by Hersman et al., in this issue.

**Table 1.** New Horizons instruments: Pluto system measurement objectives and characteristics

Instrument; PI; PC <sup>a</sup>	Measurement Objectives <sup>b</sup>	Instrument Characteristics <sup>c</sup>
Ralph MVIC; S. A. Stern (Southwest Research Institute [SwRI]), C. Olkin (SwRI), C. Howett (SwRI); Ball and SwRI	<ul style="list-style-type: none"> <li>• <b>Hemispheric panchromatic maps of Pluto and Charon at best resolution &gt;0.5 km/pixel</b></li> <li>• <b>Hemispheric four-color maps of Pluto and Charon at best resolution &gt;5 km/pixel</b></li> <li>• <b>Search for/map atmospheric hazes at a vertical resolution &lt;5 km</b></li> <li>• High-resolution panchromatic maps of the terminator region</li> <li>• Panchromatic wide-phase-angle coverage, panchromatic stereo images, orbital parameters, and bulk parameters of Pluto, Charon, Nix, and Hydra</li> <li>• Search for rings</li> <li>• Search for additional satellites</li> </ul>	<ul style="list-style-type: none"> <li>• Visible imaging</li> <li>• Bandpasses: 400–975 nm (panchromatic plus four-color filters (blue, red, methane, near-IR))</li> <li>• 7.5-cm primary mirror</li> <li>• Focal length: 65.75 cm</li> <li>• Field of view (FOV): 5.7° × 0.15° (stare, pan) or 5.7° × arbitrary (scan)</li> <li>• Instantaneous FOV (IFOV): 20 μrad/pixel</li> </ul>
Ralph LEISA; D. Jennings (Goddard Space Flight Center [GSFC]), C. Olkin (SwRI), C. Howett (SwRI); GSFC, Ball, and SwRI	<ul style="list-style-type: none"> <li>• <b>Hemispheric near-IR spectral maps of Pluto and Charon at best resolution &gt;10 km/pixel</b></li> <li>• <b>Hemispheric distributions of N<sub>2</sub>, CO, CH<sub>4</sub> on Pluto at a best resolution &gt;10 km/pixel</b></li> <li>• Surface temperature mapping of Pluto and Charon</li> <li>• Phase-angle-dependent spectral maps of Pluto and Charon</li> </ul>	<ul style="list-style-type: none"> <li>• IR spectral imaging</li> <li>• 7.5-cm primary mirror</li> <li>• Focal length: 65.75 cm</li> <li>• Bandpass: 1.25–2.50 μm, λ/δλ ≈ 240; 2.10–2.25 μm, λ/δλ ≈ 550</li> <li>• FOV: 0.9° × 0.9°</li> <li>• IFOV: 62 μrad/pixel</li> </ul>
Alice; S. A. Stern (SwRI); SwRI	<ul style="list-style-type: none"> <li>• <b>Upper atmospheric temperature and pressure profiles of Pluto</b></li> <li>• <b>Temperature and vertical temperature gradient measured to ~10% at a vertical resolution of ~100 km for atmospheric densities &gt;~10<sup>9</sup> cm<sup>-3</sup></b></li> <li>• <b>Search for atmospheric haze at a vertical resolution &lt;5 km</b></li> <li>• <b>Mole fractions of N<sub>2</sub>, CO, CH<sub>4</sub>, and Ar in Pluto's upper atmosphere</b></li> <li>• <b>Atmospheric escape rate from Pluto</b></li> <li>• Minor atmospheric species at Pluto</li> <li>• Search for an atmosphere of Charon</li> <li>• Constrain escape rate from upper atmospheric structure</li> </ul>	<ul style="list-style-type: none"> <li>• UV spectral imaging</li> <li>• Bandpass: 465–1880 Å</li> <li>• 4.0 × 4.0 cm entrance aperture</li> <li>• FOV: 4° × 0.1° plus 2° × 2°</li> <li>• Spectral resolution 1.8 Å/spectral element</li> <li>• Spatial resolution: 5 mrad/pixel</li> <li>• Airglow and solar occultation channels</li> </ul>
REX; L. Tyler (Stanford), I. Linscott (Stanford); Stanford and APL	<ul style="list-style-type: none"> <li>• <b>Temperature and pressure profiles of Pluto's atmosphere to the surface</b></li> <li>• <b>Surface number density to ±1.5%, surface temperature to ±2.2 K, and surface pressure to ±0.3 mbar</b></li> <li>• Surface brightness temperatures on Pluto and Charon</li> <li>• Masses and chords of Pluto and Charon; detect or constrain J<sub>2</sub>s</li> <li>• Detect, or place limits on, an ionosphere for Pluto</li> </ul>	<ul style="list-style-type: none"> <li>• X-band (7.182-GHz uplink, 8.438-GHz downlink)</li> <li>• Radiometry T<sub>Noise</sub> &lt; 150 K</li> <li>• Ultra-stable oscillator (USO) frequency stability</li> <li>• δf/f = 3 × 10<sup>-13</sup> over 1 s</li> </ul>
LORRI; A. Cheng (APL), H. Weaver (APL); APL and SSG Precision Optonics (since acquired by L3Harris)	<ul style="list-style-type: none"> <li>• Hemispheric panchromatic maps of Pluto and Charon at best resolution &gt;0.5 km/pixel</li> <li>• Search for atmospheric haze at a vertical resolution &lt;5 km</li> <li>• Long time base of observations, extending over 10–12 Pluto rotations</li> <li>• Panchromatic maps of the far-side hemisphere</li> <li>• High-resolution panchromatic maps of the terminator region</li> <li>• Panchromatic wide-phase-angle coverage, panchromatic stereo images, orbital parameters, and bulk parameters of Pluto, Charon, Nix, and Hydra</li> <li>• Search for satellites and rings</li> </ul>	<ul style="list-style-type: none"> <li>• Visible panchromatic images</li> <li>• Bandpass: 350–850 nm</li> <li>• 20.8-cm primary mirror</li> <li>• Focal length: 262 cm</li> <li>• FOV: 0.29° × 0.29°</li> <li>• IFOV: 5 μrad/pixel</li> <li>• Framing camera with &lt;0.3% geometrical distortion</li> </ul>
SWAP; D. McComas (Princeton); SwRI	<ul style="list-style-type: none"> <li>• <b>Atmospheric escape rate from Pluto</b></li> <li>• Solar wind velocity and density, low-energy plasma fluxes and angular distributions, and energetic particle fluxes at Pluto–Charon</li> <li>• Solar wind interaction of Pluto and Charon</li> </ul>	<ul style="list-style-type: none"> <li>• Solar wind detector</li> <li>• FOV: 276° × 10°</li> <li>• Energy range <ul style="list-style-type: none"> <li>– Electrostatic analyzer (ESA): 0.35–7.5 keV</li> <li>– Retarding potential analyzer (RPA): 0–2,000 V</li> </ul> </li> <li>• Energy resolution <ul style="list-style-type: none"> <li>– ESA: 0.085 ΔE/E</li> <li>– RPA: 0.5 V steps</li> </ul> </li> </ul>
PEPSSI; R. McNutt (APL); APL	<ul style="list-style-type: none"> <li>• Composition and density of PUIs from Pluto, which indirectly addresses the atmospheric escape rate</li> <li>• Energetic particle fluxes and angular distributions at the Pluto–Charon system</li> <li>• Solar wind interaction of Pluto and Charon</li> </ul>	<ul style="list-style-type: none"> <li>• Energetic particle detector</li> <li>• Energy range: 1 keV–1 MeV</li> <li>• FOV: 160° × 12°</li> <li>• Spatial resolution: 25° × 12°</li> <li>• Mass resolution: 2–15 amu</li> </ul>
VBSDC; M. Horányi (University of Colorado Boulder); Laboratory for Atmospheric and Space Physics at the University of Colorado Boulder	<ul style="list-style-type: none"> <li>• Trace the density of dust in the solar system along the New Horizons trajectory from Earth to Pluto and beyond</li> </ul>	<ul style="list-style-type: none"> <li>• 12 polyvinylidene fluoride (PVDF) panels to detect dust impacts and 2 control panels shielded from impacts</li> <li>• Panel area: 14.2 cm × 6.5 cm</li> <li>• Total area: 1,000 cm<sup>2</sup></li> <li>• Detection limit: m &gt; 10<sup>-12</sup> g</li> </ul>

Updated from Weaver et al. 2008.<sup>2</sup><sup>a</sup>PI, Original principal investigator. Current PI, when applicable, is in bold. PC, Primary contractor.<sup>b</sup>Group 1 measurement objectives are bold.<sup>c</sup>Instrument characteristics are summary values.

A more detailed overview of the New Horizons instrument suite is provided by Weaver et al. in *Space Science Reviews* (volume 140, 2008),<sup>2</sup> and even more extensive discussions of each instrument are provided in other articles in that same volume.<sup>3–9</sup> More recently, detailed results on the in-flight performance and calibration of MVIC<sup>10</sup> and LORRI<sup>11</sup> have been published.

Despite their relatively small size, small mass, and low power usage, the New Horizons instruments have proven to be both capable and reliable. Trending results over the entire mission, now exceeding 17 years, have shown essentially no performance degradation for either the instruments or the spacecraft subsystems. The instruments are as capable in 2023 as they were at launch in 2006, which is testimony to the extraordinary efforts of the instrument teams and their contractors in designing and building them. Even more important, the instruments and spacecraft performed flawlessly during all three of the mission's planetary flybys (Jupiter, Pluto, and Arrokoth) and returned data that are revolutionizing our understanding of the fascinating objects in the outer solar system and the processes that shaped them.

To meet the lifetime requirements, each instrument's electronics interfaced with the two redundant command and data handling (C&DH) subsystems, and three of the instruments had significant internal redundancy. These instruments were developed in the early 2000s and took advantage of the technologies of that era to meet the stringent mass and power requirements.

As New Horizons continues on its journey beyond Pluto and Arrokoth, its reliability—along with the reliability of the instrument suite—enables it to continue making substantial contributions to our understanding of the outer regions of the Kuiper Belt and the heliosphere. To better enable these measurements, a series of spacecraft and instrument software upgrades were designed and implemented in 2020–2021, as described below. These upgrades have now been demonstrated and will prove useful as the spacecraft travels even farther from our Sun during the next phase of its mission.

On the following pages, each instrument is described to provide the reader with an understanding of the basic design and performance; each description focuses on the key design elements enabling the instrument to meet the requirements in Table 1. The additional capabilities enabled by the recent software upgrades are summarized, and specific attention is paid to the reliability and stability that these instruments have exhibited from launch in 2006 to their most recent observations and in-flight calibration in 2019.

## RALPH

The Ralph instrument is mounted to the exterior of the New Horizons spacecraft,<sup>12</sup> as illustrated in Figure 2. (*Ralph* is a name, not an acronym, taken from one of

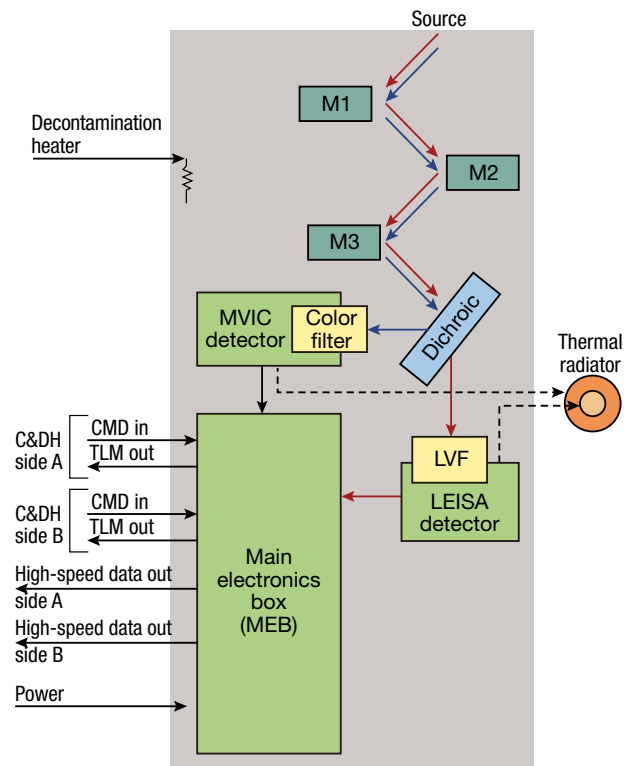


**Figure 3.** Ralph block diagram. The three-mirror anastigmatic optical system creates an image whose shorter wavelengths are reflected to the MVIC focal plane by the dichroic and whose longer wavelengths are transmitted to the LEISA focal plane by the dichroic. The signals generated by the MVIC and LEISA focal planes are transmitted to the MEB, and from there to the spacecraft memory. The focal plane detectors are thermally coupled to an external radiator to maintain the required temperature during operation. A heater is included in the design to ensure that the optical surfaces are not degraded because of contamination (e.g., due to spacecraft thruster firings) and is turned on as needed during periods when the instrument is not collecting data.

the main characters of the American television show *The Honeymooners*.) It has two assemblies, the telescope detector assembly (TDA) and the main electronics box (MEB; see Figure 3 and Table 1). The TDA consists of a single telescope that feeds two sets of focal planes, MVIC and LEISA. The telescope uses an unobscured, off-axis, three-mirror anastigmat design to achieve its broad FOV. The entire telescope assembly, including the three diamond-turned off-axis aspherical mirrors, is constructed from a single block of grain-aligned 6061-T6 aluminum. The housing, excluding the attached covers, is also diamond turned from a single aluminum block, ensuring that the system's optical performance is insensitive to temperature and that thermal gradients are minimized. A dichroic beamsplitter transmits IR wavelengths longer than 1.1  $\mu\text{m}$  to LEISA and reflects shorter wavelengths to MVIC. The highly baffled system provides excellent sensitivity, while minimizing size and mass. The in-flight temperature of the TDA

is about 220 K to reduce the conductive and radiative thermal load on the focal planes and limit the background signal at the long-wavelength end of LEISA. The inner stage of the externally mounted passive radiator cools the LEISA detector to <110 K. The outer annulus maintains the MVIC charge-coupled devices (CCDs) at temperatures below 175 K and lowers the temperature of an  $f/2.4$  cold shield for LEISA to below 190 K, again to reduce the LEISA background. The telescope provides diffraction-limited image quality over the  $5.7^\circ \times 1.0^\circ$  FOV spanned by the MVIC and LEISA arrays.

MVIC is composed of seven CCD arrays on a single substrate. It uses two of its large-format ( $5,024 \times 32$  pixel) CCD arrays, operated in time delay integration (TDI) mode, to provide panchromatic (400–975 nm) images. Four additional  $5,024 \times 32$  CCDs, combined with the appropriate filters, also operated in TDI mode, map in blue (400–550 nm), red (540–700 nm), near-IR (780–975 nm), and a narrow methane absorption band (860–910 nm). TDI operates by synchronizing the parallel transfer rate of each of the CCD's 32 rows (each 5,024 pixels wide) to the relative motion of the image across the detector's surface. The presence of 32 rows effectively increases the integration time by that same factor, allowing high signal-to-noise measurements while scanning quickly. Finally, the  $5,024 \times 128$ -element panchromatic frame-transfer array operates in staring mode.

LEISA is an IR spectral imager that creates spectral maps in the compositionally important 1.25- to 2.5- $\mu\text{m}$  shortwave IR (SWIR) spectral region. It images a scene through a wedged filter (linear variable filter, LVF<sup>13</sup>) placed about 100  $\mu\text{m}$  above a  $256 \times 256$  detector array. An image is formed on both the wedged filter and the array simultaneously. The LVF is fabricated such that the wavelength varies along one dimension, the scan direction. It is made in two segments: (1) 1.25–2.5  $\mu\text{m}$  with  $(\lambda/\delta\lambda)$  of 240 and (2) 2.1–2.25  $\mu\text{m}$  with  $(\lambda/\delta\lambda)$  of 560. LEISA forms a spectral map by scanning the  $0.9^\circ \times 0.9^\circ$  FOV across the surface in a push-broom fashion. The frame rate is synchronized to the rate of the scan, so that a frame is read out each time the image moves by the single-pixel IFOV. The difference between a LEISA scan and an MVIC TDI scan is that in LEISA, the row-to-row image motion builds up a spectrum, while in MVIC, the motion increases the signal over a single spectral interval.

Attaining the low power (6.74 W) and mass (10.67 kg) were especially important for the New Horizons mission, for which both of these resources are at a premium. The wide MVIC FOV was a strong driver for the optical system, both in terms of design and component manufacture. This was further complicated by the fact that the LEISA detector needed to operate at significantly lower temperatures than MVIC. This meant that the optical performance had to be stable over a range of temperatures since the passive system temperature was affected by pointing and other factors during operations. Ensuring that the thermal

requirements were met under all conditions was also difficult because maintaining low mass meant that there was little margin on the radiator sizes. The low-power requirement was a challenge because it meant that current levels were low, which increased the system's sensitivity to electrical noise. In addition, at the time Ralph was made, LVF fabrication was not as well defined as it is now, and obtaining an LVF with the required transmittance, spectral resolution, and out-of-band blocking required significant effort. Finally, for a long-duration mission such as New Horizons, electronics reliability was of paramount importance. To ensure that Ralph was robust, almost all the electronics are redundant with separate interfaces to the redundant C&DH subsystems.

The radiometric stability of both MVIC and LEISA has been measured by stellar observations made throughout the mission. These have shown the MVIC red, blue, and panchromatic channels to be stable to a root mean squared (RMS) value of 5% or better. The stability levels of the lower-signal-level near-IR and  $\text{CH}_4$  channels are 10% and 15%, respectively, which is still well within their requirements. LEISA stability, as measured by the median response in the 1.8- to 2- $\mu\text{m}$  spectral range, has also been at the 5% level.

## ALICE

The Alice instrument is a compact, low-cost, lightweight (4.5 kg), low-power (4.7 W) UV imaging spectrograph. The instrument incorporates an off-axis telescope feeding a Rowland-circle spectrograph with a 520–1,870  $\text{\AA}$  spectral passband. Alice provides moderate spectral and spatial resolution capabilities and a peak effective area of  $\sim 0.3 \text{ cm}^2$  (Figure 4). Light enters Alice's  $f/3$  telescope via either the main entrance aperture (called the airglow aperture, which is co-aligned with the Ralph and LORRI entrance apertures—refer to the aperture fields of view illustration in the article by Hersman et al., in this issue) or a small fixed pickoff mirror in the Alice solar occultation channel (SOCC, co-aligned with the New Horizons high-gain antenna). Light from either aperture is reflected off the  $4 \times 4$ -cm primary mirror, then passes through a slit at the entrance of the instrument's spectrograph section, is reflected then off a holographic grating, and finally is detected using a photon-counting, microchannel plate double delay line device, read out as a  $32 \times 1,024$ -element digital array. The SOCC aperture is stepped down by a factor of  $\sim 6,400$  relative to the airglow aperture to allow Alice to look directly at the Sun for solar occultations of flyby target atmospheres. The Alice entrance slit is a “lolipop” with a  $0.1^\circ \times 4^\circ$  “slot” used primarily for airglow observations and a  $2^\circ \times 2^\circ$  “box” used mainly during solar occultation observations. The point source spectral resolution is 3–6  $\text{\AA}$ , depending on wavelength, and the plate scale in the spatial dimension is  $0.27^\circ$  per pixel. During the Pluto and Charon occultation observations, the Sun

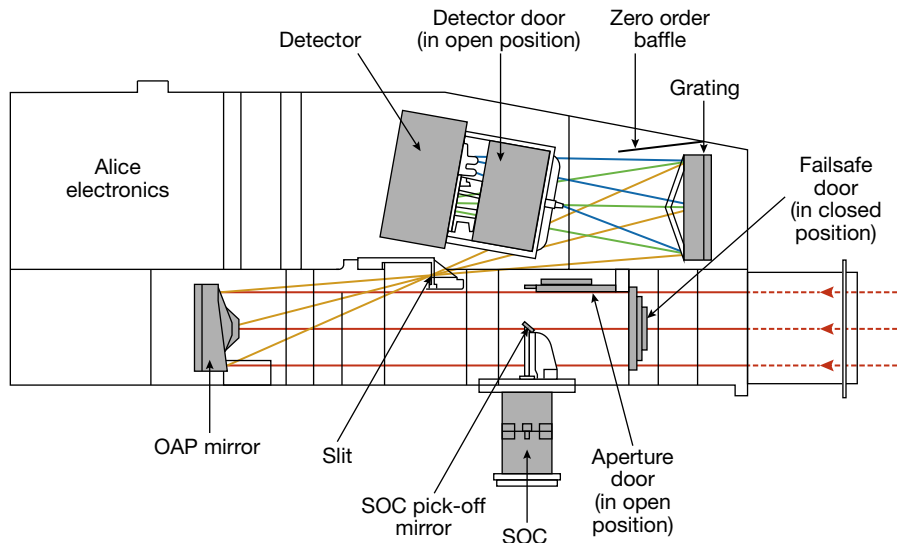


**Figure 4.** Optomechanical schematic of Alice with central-axis light rays shown. The instrument passband in the far ultraviolet is particularly susceptible to hydrocarbon contamination. The design includes several aperture doors (and a heater) to protect the instrument from contamination prior to launch and during flight.

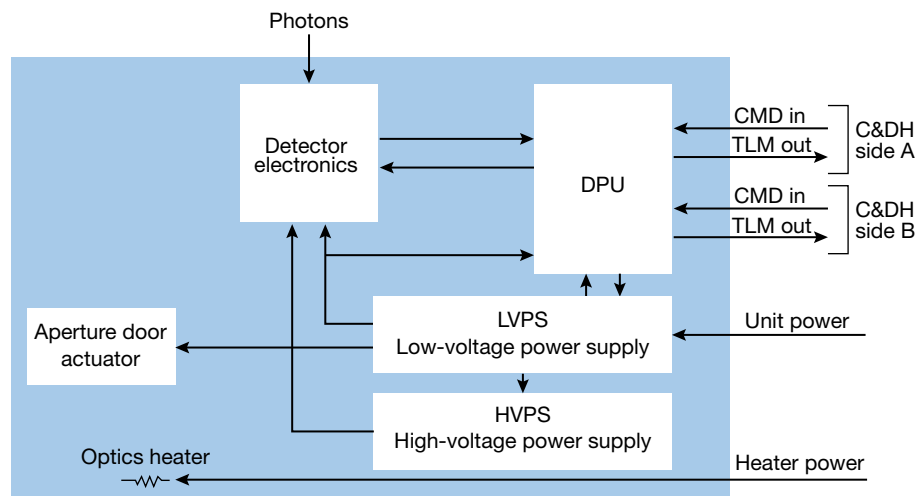


**Figure 5.** Detailed Alice instrument block diagram. UV photons striking the photodetector generate pulses that the detector electronics accumulates in a position-sensitive counter (the positions represent wavelength spectra in one dimension and spatial position in the second dimension). The instrument data processing unit (DPU) provides the interface to transmit the spectra/position data to the spacecraft for storage and downlink. The high-voltage power supply is adjustable by command to compensate for gain degradation of the detector's microchannel plates.

had an apparent diameter of  $\sim 1$  arcmin and the spectral resolution is  $3\text{--}3.5 \text{ \AA}$ . During filled-slit airglow aperture observations, the spectral resolution is  $\sim 9\text{--}10 \text{ \AA}$ . Instrument performance has been stable throughout the mission, and the instrument continues to fully function, 17+ years after launch.

The instrument electronics are internally redundant to ensure high reliability for the long duration of the mission. The internal redundancy is complemented with

independent interfaces to the redundant C&DH systems, as shown in Figure 5.

Alice is a name, not an acronym, taken from one of the main characters of the American television show *The Honeymooners*. Alice is sometimes called Pluto-Alice (P-Alice) to distinguish it from its predecessor, Rosetta-Alice (R-Alice, S. A. Stern, principal investigator), which is a similar instrument flown on the European Space Agency Rosetta mission to comet 67P//Churyumov-Gerasimenko. P-Alice has a somewhat different bandpass and various enhancements to improve reliability over R-Alice; P-Alice also includes the SOCC, which was not available on R-Alice. Both P-Alice and R-Alice are significantly improved versions of the Pluto mission HIPPS UV spectrograph (HIPPS/UVSC), which was developed at Southwest Research Institute (SwRI) in the mid-1990s with funds from NASA, the Jet Propulsion Laboratory, and SwRI (S. A. Stern, principal investigator).

Alice was designed to measure Pluto's upper atmospheric composition and temperature, which was a New Horizons Group 1 scientific objective. Alice also obtained model-dependent escape rate measurements from Pluto's atmosphere, and it provided surface reflectance results in the UV. Alice's spectral bandpass includes lines of CO, atomic H, Ar, and Ne, and the electronic bands of  $\text{N}_2$ ,  $\text{CH}_4$ , and other hydrocarbons and nitriles detectable during solar and stellar occultation observations. See Stern et al.<sup>3</sup> for further details on Alice's design and performance.

Instrument flight software allowed for modes relevant to both airglow and solar occultation studies. New flight software uplinked in 2021 allows for higher-spatial-resolution sky H Lyman- $\alpha$  mapping.

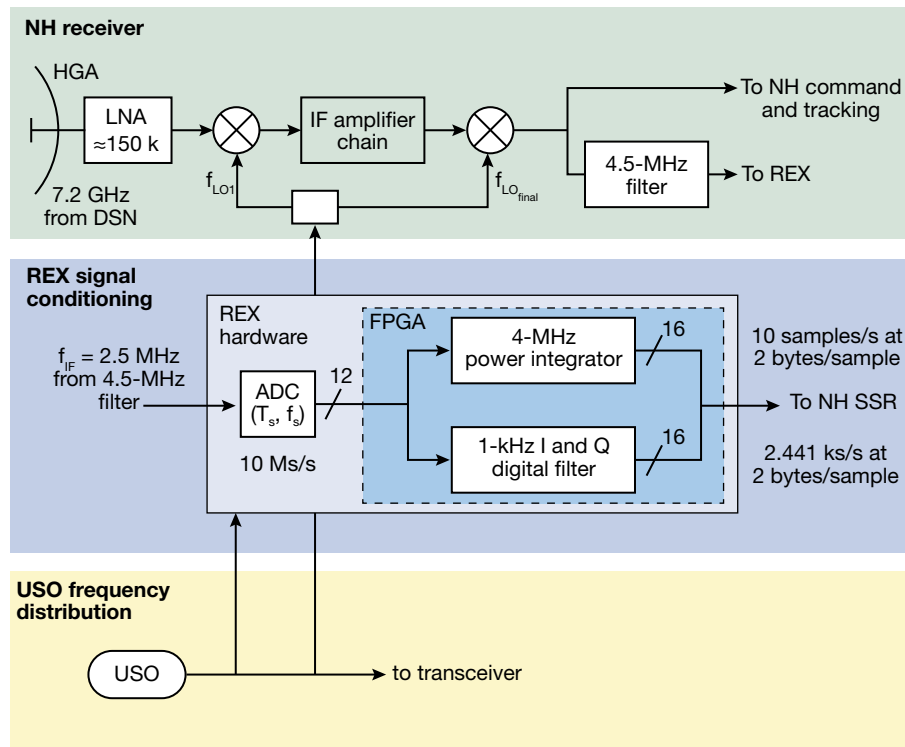


**Figure 6.** Overview of REX implementation onboard New Horizons. REX is a dual-polarization instrument for right-hand and left-hand circular polarizations. Both polarizations are implemented identically. Shown here is the common block diagram. The top section illustrates the 7.2-GHz receiver portion of the New Horizons transceiver. Radio waves illuminating the spacecraft's HGA are fed to a low-noise amplifier (LNA), then downconverted (or heterodyned), using a USO as the frequency reference, to an intermediate frequency (IF) with a 4.5-MHz bandwidth. In the middle section, the IF amplifier chain's output is input to the REX hardware embedded in the transceiver (shown in the labeled rectangle). REX signal conditioning samples the input with an analog-to-digital converter (ADC) and provides the samples to the REX gate array programmed as a digital radiometer and downconverter, converting the IF signal to baseband (i.e., 0 Hz), in a 1,250-Hz bandwidth. The filtering and decimation in the REX gate array reduces downlink data volume by the ratio of the IF to baseband bandwidth, 4.5 MHz/1.25 kHz, or 3,600 times. The radiometric process integrates RF power, providing samples at a rate of 10 per 1.024 s. The filtered data and radiometric samples are transferred to the spacecraft's solid-state recorder (SSR) for storage and later return to Earth.

## REX

The New Horizons Radio Science Experiment, REX, is unusual in that it is a collection of the spacecraft's telecommunication components operating together with a data collection, processing, and management process. The components in this ensemble perform much as individual members of an orchestra to achieve critical mission objectives, such as radio occultation, radiometric thermal measurement, bistatic radar experiments, and radio path structural characterization.

The REX instrument incorporates a small amount of signal processing hardware into the spacecraft's radio system communication and tracking functions. This architecture differs from most other US spaceflight missions that conduct occultation experiments where

radio transmissions from the spacecraft are downlinked (i.e., received on the ground). For REX, to achieve much higher signal-to-noise ratios (SNRs), the radio signals probing the structure of, for example, Pluto's atmosphere, are uplinked (i.e., signals transmitted from Earth to the New Horizons spacecraft). Because of the unusually large distance from Earth to the Pluto system, this uplink strategy with its higher SNRs was crucial to achieve the mission-required sensitivities, precision, and resolution. The architecture of the REX instrument is illustrated in Figure 6.

## LORRI

The Long Range Reconnaissance Imager (LORRI) is a panchromatic visible-light (350–850 nm) camera designed to provide high-spatial-resolution images under the low-ambient-light conditions present at the large heliocentric distances of Pluto and Arrokoth. LORRI also serves as the primary optical navigation camera on New Horizons. LORRI comprises three subsystems (Figure 7): the optical telescope assembly (OTA), the focal plane unit (FPU), and the associated support electronics (ASE). During New Horizons' launch on January 19, 2006, the OTA was protected by a one-time-open door mounted to the spacecraft. LORRI was allowed to outgas for decontamination purposes at +50°C until the door was opened on August 29, 2006. No evidence of contamination has ever been detected, and LORRI's throughput and optical performance have remained constant at the ~1% level throughout the entire mission, now in its 17th year of successful operations.

The OTA was provided by SSG Precision Optonics (since acquired by L3Harris) and is made of silicon carbide (SiC) for athermal operation; the in-flight OTA temperature has been within a few degrees of -70°C ever since the door was opened. The OTA has a Ritchey–Chrétien optical design with a three-element flat-fielding lens assembly to minimize geometrical

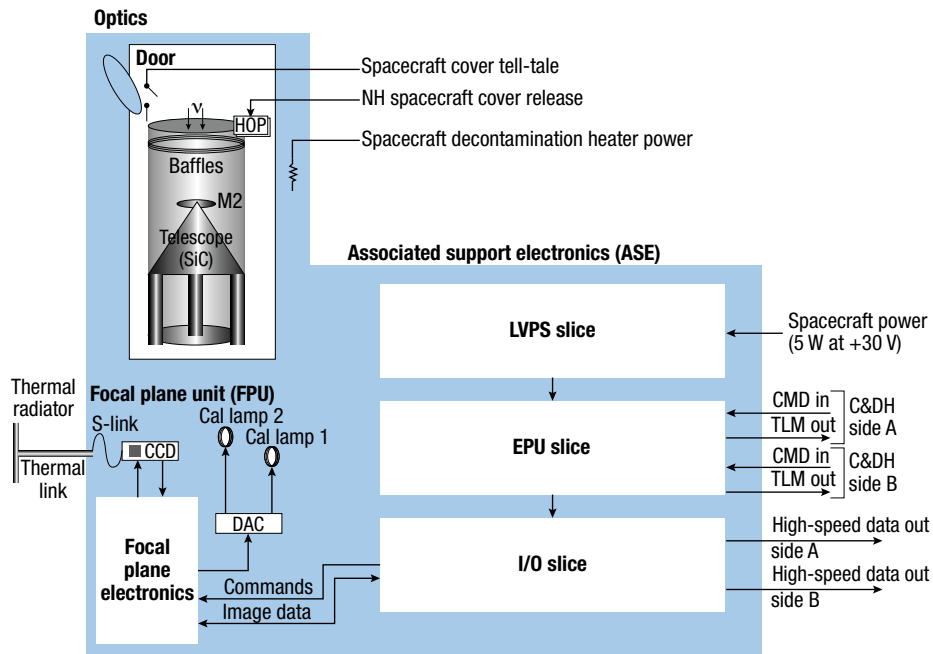


**Figure 7.** LORRI block diagram. This block diagram shows LORRI’s three main components: the OTA with its once-open door mounted to the spacecraft and the HOP paraffin actuator for deployment; the FPU with a CCD, its electronics, two tungsten filament calibration lamps, and a thermal link to a radiator for cooling the CCD; and the ASE. The ASE has three boards (“slices”): one that produces stable voltages for other components; another board with a processor that runs the LORRI flight software and receives and executes commands from the spacecraft; and an imager input/output board that processes data from the FPU and transmits data to the spacecraft. As with Ralph and Alice, LORRI includes a heater to ensure the instrument optics remain free from spacecraft contamination; it is used in a similar manner to those of the other instruments.

distortion ( $<0.3\%$  along the full FOV of 5 mrad). The OTA primary mirror has a relatively large diameter of 20.8 cm to provide both high angular resolution (5  $\mu\text{rad}/\text{pixel}$ ) and high sensitivity. LORRI can achieve an SNR of 5 on an unresolved target having a visual magnitude ( $V$ ) of  $\approx 22$  by combining  $\sim 25$  images using its longest exposure time (64.967 s). LORRI is also able to probe down to diffuse surface reflectance values of  $I/F = 0.005$  with SNR = 5 at Pluto’s heliocentric distance using a typical exposure time of only 100 ms.

The FPU has a high quantum efficiency (QE,  $\sim 90\%$  at peak), backside-illuminated, back-thinned, frame-transfer CCD detector (model CCD47-20 from e2V, now Teledyne e2V) with a  $1024 \times 1024$ -pixel optically active area (“ $1 \times 1$ ” format) that can be re-binned during readout to  $256 \times 256$  pixels (“ $4 \times 4$ ” format) for maximum sensitivity on unresolved targets. The analog signal output from the CCD is processed using correlated double-sampling and converted to data numbers (DN) using a 12-bit ADC. The electronics noise is  $\sim 1.1$  DN, and the bias level is  $\sim 540$  DN, providing a single image dynamic range of  $\sim 3,200$ . Two small tungsten filament lamps mounted near the CCD are used to test basic CCD functionality and monitor any changes in debris

on the CCD (no change has ever been seen).

The ASE has three electronics boards: one provides stable voltage outputs; one has a processor and memory for storing and executing the flight software; and one processes the output from the FPU, creates a 32-bin histogram of the digitized CCD stream, and passes the CCD image data and ancillary information to the New Horizons C&DH system, which stores all data in its 64-Gbit SSR. The C&DH system also reformats the LORRI data for downlink telemetry to Earth.

Several upgrades to LORRI’s capabilities have been made during the mission. A special “trigger mode” capability, whereby LORRI can autonomously detect a target and start taking images, was designed, developed, and ground-tested in 2012–2013. We expected to use trigger mode to save data volume as the spacecraft

scanned LORRI’s boresight across Pluto’s large pointing error ellipse, producing many blank images, but because we could not perform good in-flight tests on an extended target, trigger mode was not used during the Pluto flyby. The LORRI flight software was upgraded in 2019 to increase the maximum available exposure time from 29.967 s to 64.967 s, and this capability has been used extensively ever since. In 2020, New Horizons’ C&DH flight software was upgraded to enable onboard coadding of up to 100 LORRI  $4 \times 4$ -format images, which could be used to save precious SSR data volume.

## SWAP

The Solar Wind Around Pluto (SWAP) instrument<sup>7</sup> was designed to measure the solar wind at large distances from the Sun and its interaction with Pluto, including Pluto-generated PUIs.<sup>14</sup> Because of the great heliocentric distances and large range of viewing directions, SWAP was designed to have extremely high sensitivity, a very large FOV, and very low backgrounds. These attributes allowed SWAP to make unprecedented measurements of Pluto’s interaction with the solar wind,<sup>15</sup> as well as unique measurements of the Jovian



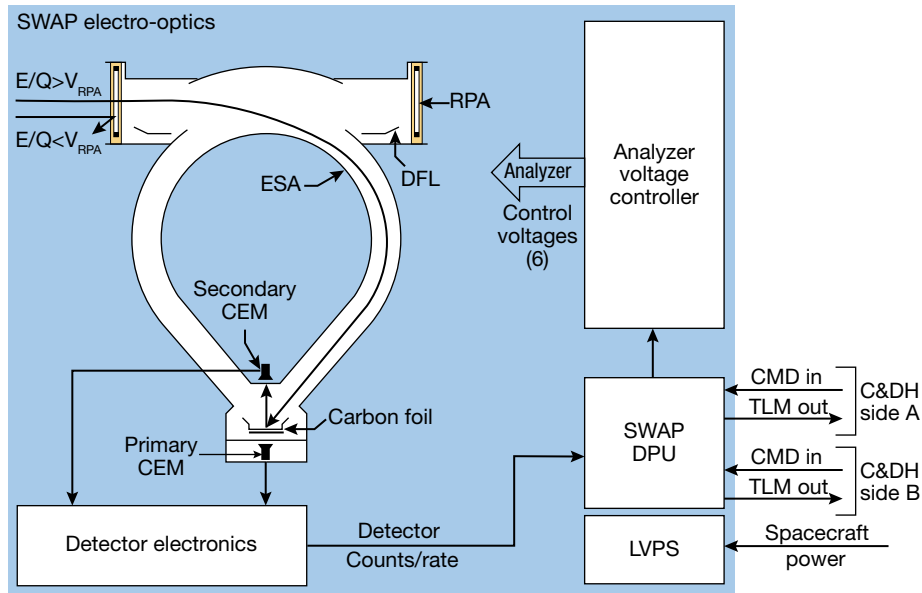


**Figure 8.** Schematic diagram of the SWAP instrument: the electro-optics (including the RPA, deflector, and detector assembly) and associated electronics. Collectively, these elements select the angles and energies of the solar wind and PUIs to be measured. The analyzer voltages sweep through a range that filters the incoming particles such that only a select band based on their energy level and direction reaches the detector at any one setting of the voltage range. (Adapted from McComas et al.<sup>7</sup>)

magnetotail to  $>2,500 R_J^{16}$  and fundamental observations of interstellar PUIs.<sup>17</sup> SWAP continues to make excellent observations of the solar wind and interstellar PUIs, now out past 53 au.<sup>18</sup>

Figure 8 schematically depicts SWAP's principal electro-optics: (1) an RPA, (2) a deflector (DFL), and (3) an electrostatic analyzer (ESA). Collectively, these elements select the angles and energies of the solar wind and PUIs to be measured. Ions with energy per charge ( $E/q$ ) greater than the RPA voltage enter through the RPA. The RPA protected SWAP from the very high

solar wind fluxes in the inner heliosphere; beyond Jupiter the RPA was generally left off. The ESA provides energy selection and rejects ions outside the selected  $E/q$  range. It also protects the detectors from UV light and neutral particles. Ions selected by the ESA are registered with a coincidence detector system. The voltage on the ESA varies from 0 to  $-4,000$  V, enabling it to select particles from  $35$  eV/ $q$  to  $7.5$  keV/ $q$  with a  $\Delta E/E$  of 8.5% FWHM.

Figure 9 compares SWAP's energy-angle response function for a 1-keV proton beam (left) with a SIMION model (right). The energy and angle binning in the SIMION model was set to the same values as in the instrument for a better comparison. The figure shows the excellent agreement between the modeling and the calibration measurements with the ion beam. (From McComas et al.<sup>7</sup>)

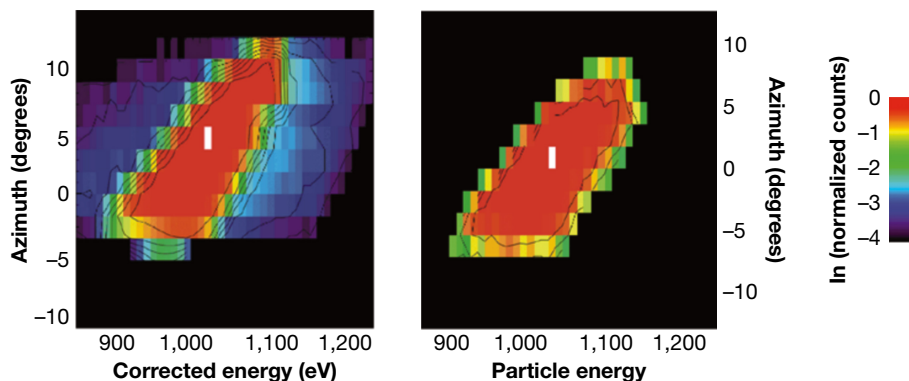


**Figure 9.** Comparison of SWAP's energy-angle response function for a 1-keV proton beam (left) and the ion simulation (right). The energy and angle binning in the SIMION model was set to the same values as in the instrument for a better comparison. The figure shows the excellent agreement between the modeling and the calibration measurements with the ion beam. (From McComas et al.<sup>7</sup>)

SIMION model was set to the same values as in the instrument for a better comparison. Clearly, there is an excellent agreement between the modeling and the calibration measurements with the ion beam.

On February 19, 2021, a simple flight software upgrade redefined the internal formatting of a large daily histogram into 47 sequential (~30-min) histograms with normal 64-step energy resolution and started producing the high-cadence data product. This enabled measurements of individual solar wind and PUI distributions nearly 50 times faster than the 1-day distributions previously collected. This time resolution is sufficient to resolve the shock structures and quantify the particle heating across the shock (see McComas et al.<sup>18</sup> for details and for SWAP's current configuration and capabilities). The new high-resolution observations are important for understanding shocks in the outer heliosphere, the heliospheric termination shock, and more broadly for PUI-mediated shocks across many astrophysical systems.

## PEPSSI

The PEPSSI (Pluto Energetic Particle Spectrometer Science Investigation) experiment<sup>7</sup> was designed to measure suprathermal ions and energetic particles associated with neutral gas escaping from Pluto's atmosphere and monitor the radiation environment (e.g., in the solar wind, ionosphere, magnetotail, or their analogues) on approach to and departure from the Pluto–Charon system. PEPSSI is from the first generation of low-mass (<1.48 kg), low-power (2.49 W), time-of-flight (TOF)

mass spectrometers<sup>19</sup>—called *pucks* (from their roughly hockey-puck-sized TOF chambers)—designed and built at APL and flown to five worlds: three orbital missions, to Mercury, Earth, and Jupiter; and the flybys of Jupiter, Pluto, and Arrokoth by New Horizons. PEPSSI originally had a prime energy range of ~15 keV to 1 MeV, but we have since extended the usable, calibrated energy range to lower<sup>20</sup> and higher<sup>21</sup> energies, adding  $\geq 2$  keV/nuc ions (e.g., interstellar PUIs) and ~70 MeV to >1.4 GeV ions (e.g., galactic cosmic rays), respectively, to its capabilities. Laboratory measurements with the PEPSSI engineering model were made from 2016 to 2018 in support of this effort to broaden the impact of the flight unit's scientific measurements.

Like other TOF mass spectrometers, PEPSSI uses TOF measurements in combination with kinetic energy measurements from silicon solid-state detectors (SSDs), as illustrated in Figure 10. The TOF measurements rely on thin “start” and “stop” foils to time the primary ion's flight between the two foils, resulting in a velocity measurement (including six sectors of angular sensitivity). The primary (desired foreground) ions pass through the foils, producing secondary electrons that are electrostatically steered toward a microchannel plate for detection (via an electron avalanche process). The energy is determined when the primary ion enters the active volume of the SSD and Coulomb collisions liberate electrons from ions in the Si crystal lattice, which is biased by a voltage sufficient to separate the resulting electron-hole pairs. In combination with many such electron-hole pairs (released in a quantity roughly proportional to  $E$  since

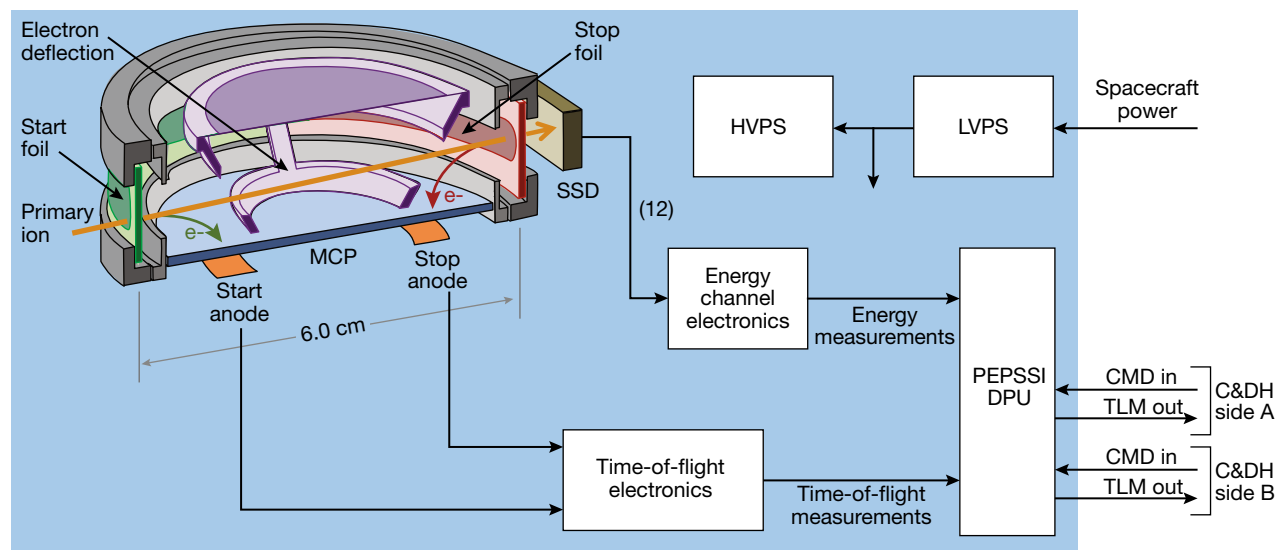


**Figure 10.** Measurement method for PEPSSI's prime “triple coincidence” (TOF vs. E) detection mode. The PEPSSI instrument is depicted in cross section with colored arrows representing charged particles as the primary ion (orange) passes first through the  $10\text{-}\mu\text{g}/\text{cm}^2$  start foil and then the  $19\text{-}\mu\text{g}/\text{cm}^2$  stop foil, resulting in emitted secondary electrons from the start (green) and stop (red) sides of the TOF chamber, providing a velocity measurement. Then the primary ion is stopped inside the  $500\text{-}\mu\text{m}$ -thick silicon SSD, where the kinetic energy is detected. The signals from the detector are processed by the PEPSSI electronics to provide composition and energy data (refer to Figure 13 in the article by Weaver et al., in this issue). (Adapted from Clark et al.<sup>19</sup>)

the ion stops in the SSD, due to the many collisions, releasing all of its kinetic energy), a pulse is produced that is analyzed and calibrated to energy. Together, the measured kinetic energy,  $E$ , and velocity,  $v$ , are the quantities needed to determine the primary ion's mass,  $m$ , as illustrated by the nonrelativistic expression  $E = \frac{1}{2}mv^2$ .

In addition to making Pluto observations,<sup>22,23</sup> as New Horizons flew through Jupiter's magnetosphere in 2007,<sup>24</sup> PEPSSI made measurements during the  $>2,500 R_J$  (Jovian radius,  $R_J = 71,400$  km) traversal of the Jovian magnetotail. For example, it measured dispersive ion flows in filamentary structures<sup>25</sup> and intruding interplanetary He ions.<sup>26</sup> PEPSSI also made observations during the Arrokoth flyby,<sup>27</sup> finding conditions consistent with its years of interplanetary measurements.<sup>18,19</sup>

More recently, the PEPSSI team conducted a major flight software update on April 10, 2022. The primary goal of the update was to add a "shock" burst capability to permit an autonomously detected particle event (observed via a jump in a counting rate relative to a long average) to trigger the circularly buffering high-time-resolution (e.g., 20 s) data, covering  $\sim 1.5$  days before the trigger, to be packetized and sent to the New Horizons SSR. The trigger also increases the data rate to a much higher cadence (e.g., 20 s versus 240 s) for an interval of  $\sim 2$  days after the trigger. (Illustrative, nominal setting values are provided here, but are commandable, with constraints.) Together, these updates will allow the limited data volume to be concentrated more on events of high scientific interest, making more efficient use of spacecraft and Deep Space Network resources and thus resulting in a higher science return from PEPSSI and New Horizons.

PEPSSI operations remain nominal and robust. Despite the instrument aperture misalignment during spacecraft assembly (refer to section 5.1.1 of McNutt et al.<sup>7</sup>), PEPSSI has achieved all science requirements at Pluto and Arrokoth, produced significant new insights into the properties of Jupiter's magnetotail following the early gravity assist at that planet, and continues to provide new and novel measurements of pickup and suprathermal ions in the far solar wind near the plane of the ecliptic (New Horizons and Voyager 2 remain at approximately the same heliolongitudes, but Voyager 2 is  $\sim 50^\circ$  south of the plane of the ecliptic and Voyager 1  $35^\circ$  to the north; refer to Figure 35 in McNutt et al.<sup>7</sup>)

The power supplies and associated voltages and currents remain solidly within launch specifications and continue to be steady. This is also true for the various telemetered temperature values. In coming in and out of lengthy (multiple-month) hibernation periods without direct contact with Earth, PEPSSI continues to operate nominally. Between 2007 and early 2013, there were multiple periods during which the instrument was powered down and left off. Following the Pluto flyby, the instrument has typically been left powered up to take near-continuous data, and this continues

to be the case. There have been no adverse effects in instrument operation.

There has been no observed difference in engineering parameters whether in spin-stabilized or three-axis-stabilized mode. From commissioning in 2006 through 2022, the instrument had undergone  $\sim 180$  power cycles and  $\sim 50$  EEPROM writes.

The efficiency of PEPSSI is time dependent, likely due to charging up of the foils. The start foil uses aluminum that forms an insulating oxide layer so that secondary electrons released by the primary ions are not quickly replenished, so the resulting charging reduces the secondary electron yield and, therefore, the ion detection efficiency. The charge can equilibrate and the efficiency recovers when the high voltage is turned off (e.g., during power cycles). That behavior occurs in-flight on the timescale of months and is tracked and corrected in flight by using a small, degraded Am-241 calibration source (Appendix A of Kollmann et al.<sup>19</sup>).

The design heritage of PEPSSI and the other pucks continues with the latest APL TOF-mass-spectrometer in space, EPI-Lo (Energetic Particle Instrument – Low Energy). This instrument uses the "mushroom" design<sup>28</sup> and comprises half of the Princeton-led ISOIS energetic particle investigation<sup>29</sup> instrument suite on NASA's APL-led Parker Solar Probe mission to the Sun.<sup>30,31</sup>

## VBSDC

New Horizons is the first planetary mission to carry a student-built instrument. The Venetia Burney Student Dust Counter (VBSDC) experiment is an impact dust detector designed to map the spatial and size distribution of dust along the trajectory of the spacecraft across the solar system. The instrument was initially called the Student Dust Counter (SDC), but in 2006, it was named for Venetia Burney, who as a child offered the name Pluto for the newly discovered ninth planet in 1930. The sensors are thin ( $28 \mu\text{m}$ ), permanently polarized PVDF plastic films generating an electrical signal when dust particles penetrate their surface. VBSDC has a total sensitive surface area of  $\sim 0.1 \text{ m}^2$ , pointing most of the time close to the ram direction of the spacecraft. VBSDC can detect particles with masses greater than  $10^{-12} \text{ g}$ . The instrument was designed, built, tested, and integrated by students. As of this writing, seven generations of graduate students have been involved in operating VBSDC.

The VBSDC electronics are carried on two multi-layer printed wiring assemblies (PWAs) housed in the VBSDC electronics box. Signals from the detectors come through an intra-harness onto the analog PWA where they are amplified, conditioned, and converted to digital data. The digital data are collected to registers in the field-programmable gate array (FPGA) on the digital PWA (Figure 11), and from there to the microprocessor, which adds timestamps to the data and stores them

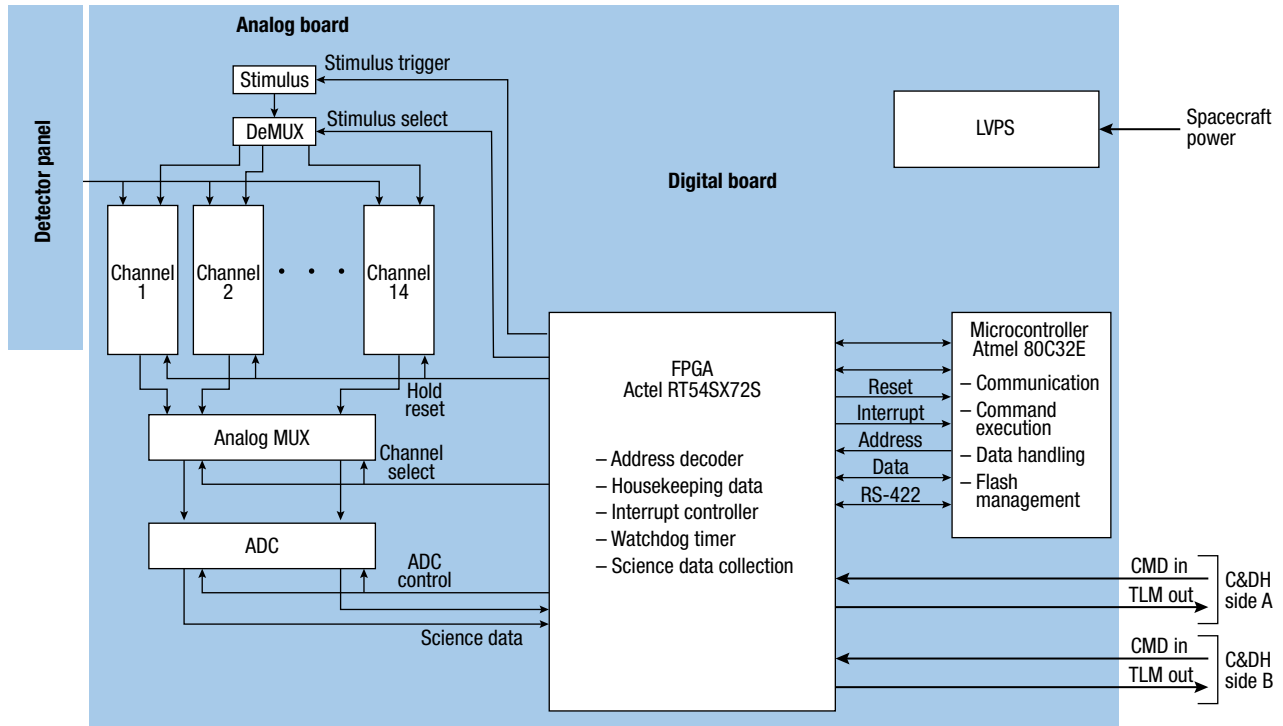


**Figure 11.** VBSDC electronics block diagram. Signals from the PVDF detectors are routed to individual analog electronics chains. Under FPGA control, the science and housekeeping data are collected and passed to the system microprocessor to manage long-term storage of data into flash memory. The FPGA also acts as a switch between the redundant spacecraft communications lines and the microprocessor.

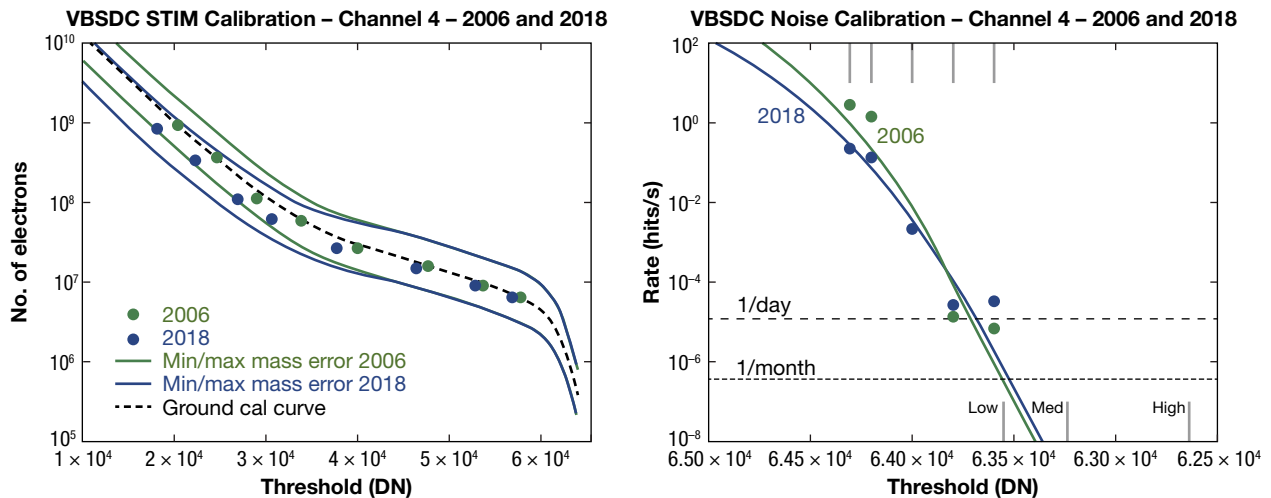


**Figure 12.** Onboard calibration stimulus test results. Left, Stimulus tests of channel 4 in 2006, 2018, and the preflight calibration curve. Right, VBSDC channel 4 noise collected in 2006 and 2018 using a noise floor calibration routine. The curves are fit to the collected rates at five separate thresholds (marked on the upper horizontal axis). The science collection thresholds (labeled Low, Med, and High on the right-hand panel) are also indicated. VBSDC can autonomously raise and lower its science thresholds for each channel during noisy periods. DN, digital number.

in long-term, nonvolatile memory. The digital PWA also contains the power supply, system health monitoring circuitry, and interface electronics for spacecraft communications.

While the spacecraft remains in hibernation for long periods of time, VBSDC remains on and collects data.

It is preprogrammed to execute a self-checkout prior to a scheduled spacecraft ground contact to transmit its status. The VBSDC flight software manages the setup and data collection of the onboard calibration stimulus tests (Figure 12). It also performs a noise floor calibration. This consists of changing the thresholds of all

the channels to a series of levels sensitive enough that electronics noise becomes detectable. By counting the number of science interrupts (“dust hits”) obtained at each threshold over specified times, the statistical distribution of the noise on each channel can be calculated (Figure 12). The flight software allows for up to five levels and test times. The test thresholds are configurable from the ground, but the durations are permanently set.

VBSDC has remained remarkably stable since launch, as indicated by both its onboard calibration and instrument noise checkouts (Figure 12), and it should continue to contribute to the New Horizons science results for many years to come.

## SUMMARY

The New Horizons instrument suite has demonstrated excellent performance, returning a set of data meeting the requirements for full mission success. The instruments continue to be fully operational after 17 years of flight as of the date of this publication and give every evidence of being capable of excellent performance well into the future.

**ACKNOWLEDGMENTS:** The success of New Horizons’ instruments is a testament to the skill and dedication of the instrument team members who developed them under stringent schedule demands. Work on the New Horizons mission was performed under NASA contracts NAS5-97271/TO30 (APL) and NASW-02008 (SwRI).

## REFERENCES AND NOTES

- <sup>1</sup>The reliability requirement was defined by a probability of success of 85% after 16 years for full mission success because the flight time to Pluto could be much longer if the actual launch was at the end of the launch window in 2006 or delayed until 2007 (see Fountain et al.<sup>12</sup>).
- <sup>2</sup>H. A. Weaver, W. C. Gibson, M. B. Tapley, L. A. Young, and S. A. Stern, “Overview of the New Horizons science payload,” *Space Sci. Rev.*, vol. 140, pp. 75–91, 2008, <https://doi.org/10.1007/s11214-008-9376-6>.
- <sup>3</sup>D. C. Reuter, S. A. Stern, J. Scherrer, D. E. Jennings, J. W. Baer, et al., “Ralph: A visible/infrared imager for the New Horizons Pluto/Kuiper Belt mission,” *Space Sci. Rev.*, vol. 140, pp. 129–154, 2008, <https://doi.org/10.1007/s11214-008-9375-7>.
- <sup>4</sup>S. A. Stern, D. C. Slater, J. Scherrer, J. Stone, G. Dirks, et al., “ALICE: The ultraviolet imaging spectrograph aboard the New Horizons Pluto-Kuiper Belt mission,” *Space Sci. Rev.*, vol. 140, pp. 155–187, 2008, <https://doi.org/10.1007/s11214-008-9407-3>.
- <sup>5</sup>G. L. Tyler, I. R. Linscott, M. K. Bird, D. P. Hinson, D. F. Strobel, et al., “The New Horizons Radio Science Experiment (REX),” *Space Sci. Rev.*, vol. 140, pp. 217–259, 2008, <https://doi.org/10.1007/s11214-007-9302-3>.
- <sup>6</sup>A. F. Cheng, and 15 coauthors, “Long-Range Reconnaissance Imager on New Horizons,” *Space Sci. Rev.*, vol. 140, pp. 189–215, 2008, <https://doi.org/10.1007/s11214-007-9271-6>.
- <sup>7</sup>D. McComas, F. Allegrini, F. Bagenal, P. Casey, P. Delamere, et al., “The Solar Wind Around Pluto (SWAP) instrument aboard New Horizons,” *Space Sci. Rev.*, vol. 140, pp. 261–313, 2008, <https://doi.org/10.1007/s11214-007-9205-3>.
- <sup>8</sup>R. L. McNutt, S. A. Livi, R. S. Gurnee, M. E. Hill, K. A. Cooper, et al., “The Pluto Energetic Particle Spectrometer Science Investigation (PEPSSI) on New Horizons,” *Space Sci. Rev.*, vol. 140, pp. 315–385, 2008, <https://doi.org/10.1007/s11214-008-9436-y>. Erratum vol. 145, p. 381, 2009, <https://doi.org/10.1007/s11214-009-9534-5>.

- <sup>9</sup>M. Horányi, V. Hoxie, D. James, A. Poppe, C. Bryant, et al., “The Student Dust Counter on the New Horizons mission,” *Space Sci. Rev.*, vol. 140, pp. 387–402, 2008, <https://doi.org/10.1007/s11214-007-9250-y>.
- <sup>10</sup>C. J. A. Howett, A. H. Parker, C. B. Olkin, D. C. Reuter, K. Ennico, et al., “Inflight radiometric calibration of New Horizons’ Multispectral Visible Imaging Camera (MVIC),” *Icarus*, vol. 287, pp. 140–151, 2017, <https://doi.org/10.1016/j.icarus.2016.12.007>.
- <sup>11</sup>H. A. Weaver, A. F. Cheng, F. Morgan, H. W. Taylor, S. J. Conard, et al., “In-flight performance and calibration of the LOng Range Reconnaissance Imager (LORRI) for the New Horizons mission,” *Pub. Astron. Soc. Pacific*, vol. 132, no. 1009, article 035003, 2020, <https://doi.org/10.1088/1538-3873/ab67ec>.
- <sup>12</sup>G. H. Fountain, D. Y. Kusnierkiewicz, C. B. Hersman, T. S. Herder, T. B. Coughlin, et al., “The New Horizons spacecraft,” in *The New Horizons Spacecraft, New Horizons – Reconnaissance of the Pluto-Charon System and the Kuiper Belt*, C. T. Russell Ed. Springer, Netherlands, 2009, pp. 23–47.
- <sup>13</sup>K. P. Rosenberg, K. D. Hendrix, D. E. Jennings, D. C. Reuter, M. D. Jhabvala, and A. T. La, “Logarithmically variable infrared etalon filters,” in *SPIE Proc. vol. 2262, Optical Thin Films IV: New Developments*, July 25–27, 1994, <https://doi.org/10.1117/12.185804>.
- <sup>14</sup>D. J. McComas, H. A. Elliott, and N. A. Schwadron, “Pickup hydrogen distributions in the solar wind at ~11 AU: Do we understand pickup ions in the outer heliosphere?” *J. Geophys. Res.*, vol. 115, no. A3, article A03102, 2010, <https://doi.org/10.1029/2009JA014604>.
- <sup>15</sup>D. J. McComas, H. A. Elliott, S. Weidner, P. Valek, E. J. Zirnstein, et al., “Pluto’s interaction with the solar wind,” *J. Geophys. Res. Space Phys.*, vol. 121, no. 5, pp. 4232–4246, 2016, <https://doi.org/10.1002/2016JA022599>.
- <sup>16</sup>D. J. McComas, F. Allegrini, F. Bagenal, F. Crary, R. W. Ebert, et al., “Diverse plasma populations and structures in Jupiter’s magnetotail,” *Science*, vol. 318, no. 5848, pp. 217–220, 2007, <https://doi.org/10.1126/science.1147393>.
- <sup>17</sup>D. J. McComas, P. Swaczyna, J. R. Szalay, E. J. Zirnstein, J. S. Rankin, et al., “Interstellar pickup ion observations halfway to the termination shock,” *Astrophys. J. Supp. Ser.*, vol. 254, no. 19, pp. 1–17, 2021, <https://doi.org/10.3847/1538-4365/abee76>, and references therein.
- <sup>18</sup>D. J. McComas, B. L. Shrestha, P. Swaczyna, J. S. Rankin, S. E. Weidner, et al., “First high-resolution observations of interstellar pickup ion mediated shocks in the outer heliosphere,” *Astro. Phys. J.*, vol. 934, no. 147, pp. 1–22, 2022, <https://doi.org/10.3847/1538-4357/ac7956>.
- <sup>19</sup>G. Clark, I. Cohen, J. H. Westlake, G. B. Andrews, P. Brandt, et al., “The ‘Puck’ energetic charged particle detector: Design, heritage, and advancements,” *J. Geophys. Res.*, vol. 121, no. 8, pp. 7900–7913, 2016, <https://doi.org/10.1002/2016JA022579>.
- <sup>20</sup>P. Kollmann, M. E. Hill, R. L. McNutt Jr., L. E. Brown, R. C. Allen, et al., “Suprathermal ions in the outer heliosphere,” *Astrophys. J.*, vol. 876, no. 1, art. 46, 2019, <https://doi.org/10.3847/1538-4357/ab125f>.
- <sup>21</sup>M. E. Hill, R. C. Allen, P. Kollmann, L. E. Brown, R. B. Decker, et al., “Influence of solar disturbances on galactic cosmic rays in the solar wind, heliosheath, and Local Interstellar Medium: Advanced Composition Explorer, New Horizons, and Voyager observations,” *Astrophys. J.*, vol. 905, no. 1, art. 69, 2020, <https://doi.org/10.3847/1538-4357/abb408>.
- <sup>22</sup>F. Bagenal, M. Horányi, D. J. McComas, R. L. McNutt Jr., H. A. Elliott, et al., “Pluto’s interaction with its space environment: Solar wind, energetic particles, and dust,” *Science*, vol. 351, art. aad9045, 2016, <https://doi.org/10.1126/science.aad9045>.
- <sup>23</sup>P. Kollmann, M. E. Hill, R. C. Allen, R. L. McNutt Jr., L. E. Brown, et al., “Pluto’s interaction with energetic heliospheric ions,” *J. Geophys. Res.*, vol. 124, no. 9, pp. 7413–7424, 2019, <https://doi.org/10.1029/2019JA026830>.
- <sup>24</sup>R. L. McNutt Jr., D. K. Haggerty, M. E. Hill, S. M. Krimigis, S. Livi, et al., “Energetic particles in the Jovian magnetotail,” *Science*, vol. 318, no. 5848, pp. 220–222 (2007), <https://doi.org/10.1126/science.1148025>.
- <sup>25</sup>M. E. Hill, D. K. Haggerty, R. L. McNutt Jr., and C. P. Paranicas, “Energetic particle evidence for magnetic filaments in Jupiter’s magnetotail,” *J. Geophys. Res.*, vol. 114, no. A11, art. A11201, 2009, <https://doi.org/10.1029/2009JA014374>.
- <sup>26</sup>D. K. Haggerty, M. E. Hill, R. L. McNutt Jr., and C. P. Paranicas, “Composition of energetic particles in the Jovian magnetotail,” *J. Geophys. Res.*, vol. 114, no. A2, art. A02208, 2009, <https://doi.org/10.1029/2008JA013659>.

- <sup>27</sup>S. A. Stern, H. A. Weaver, J. R. Spencer, C. B. Olkin, G. R. Gladstone, et al., “Initial results from the New Horizons exploration of 2014 MU69, a small Kuiper Belt object,” *Science*, vol. 364, no. 6441, art. eaaw9771, 2019, <https://doi.org/10.1126/science.aaw9771>.
- <sup>28</sup>M. E. Hill, D. G. Mitchell, G. B. Andrews, S. A. Cooper, R. S. Gurnee, et al., “The Mushroom: A half-sky energetic ion and electron detector,” *J. Geophys. Res.*, vol. 122, no. 2, pp. 1513–1530, 2017, <https://doi.org/10.1002/2016JA022614>.
- <sup>29</sup>D. J. McComas, N. Alexander, N. Angold, S. Bale, C. Beebe, et al., “Integrated Science Investigation of the Sun (ISIS): Design of the

- Energetic Particle Investigation,” *Space Sci. Rev.*, vol. 204, pp. 187–256, 2016, <https://doi.org/10.1007/s11214-014-0059-1>.
- <sup>30</sup>N. J. Fox, M. C. Velli, S. D. Bale, R. Decker, A. Driesman, et al., “The Solar Probe Plus Mission: Humanity’s first visit to our star,” *Space Sci. Rev.*, vol. 204, pp. 7–48, 2016, <https://doi.org/10.1007/s11214-015-0211-6>.
- <sup>31</sup>J. Kinnison, M. K. Lockwood, N. J. Fox, R. Conde, and A. Driesman, “Solar Probe Plus: A mission to touch the sun,” in *Proc. 2013 IEEE Aerosp. Conf.*, Big Sky, MT, 2013, pp. 1-11, <https://doi.org/10.1109/AERO.2013.6496957>.



**Glen H. Fountain**, Space Exploration Sector, Johns Hopkins University Applied Physics Laboratory, Laurel, MD

Glen H. Fountain is a program manager in APL’s Space Exploration Sector. He received a BS and an MS in electrical engineering from Kansas State University. During his early career, he was a member of

teams that developed a number of space missions for both the Department of Defense and NASA. From 1974 on, he has held a number of line and project management positions in APL’s Space Department (now Space Exploration Sector). From 2004 through 2015, he was the project manager of the New Horizons mission. He has been recognized for his work in various ways, among them the American Institute of Aeronautics and Astronautics (AIAA) Von Braun Award for outstanding space program management (2007), NASA Exceptional Public Service Medals (2008, 2016), and the Space X/AIAA Award for technical excellence (2015). His email address is [glen.fountain@jhuapl.edu](mailto:glen.fountain@jhuapl.edu).



**Harold A. Weaver**, Space Exploration Sector, Johns Hopkins University Applied Physics Laboratory, Laurel, MD

Harold A. Weaver is a scientist in APL’s Space Exploration Sector. He received a BS in physics from Duke University and an MS and a PhD in physics from Johns Hopkins University. Hal was the project scientist on NASA’s New Horizons (NH) mission during 2003–2022 and the principal investigator (PI) of NH’s Long Range Reconnaissance Imager (LORRI) during 2016–2022, and he has been an NH science co-investigator (CoI) since 2003. He also served as the PI of the LORRI instrument on NASA’s Lucy mission from 2017 to 2022. He has been pursuing space-borne, rocket-borne, and ground-based investigations in planetary science since 1978. Hal received the NASA Medal for Exceptional Scientific Achievement in 1988 for his role in discovering water emissions from Comet Halley using NASA’s Kuiper Airborne Observatory. He has led multiple investigations of comets using the International Ultraviolet Explorer, the Hubble Space Telescope, and the Far Ultraviolet Spectroscopic Explorer, and he was a CoI on the Rosetta-Alice instrument. In 2005, Hal co-led the team that discovered two small satellites of Pluto (Nix and Hydra). He is a fellow of the American Astronomical Society and a full member of the International Academy of Astronautics. His email address is [hal.weaver@jhuapl.edu](mailto:hal.weaver@jhuapl.edu).

Hal received the NASA Medal for Exceptional Scientific Achievement in 1988 for his role in discovering water emissions from Comet Halley using NASA’s Kuiper Airborne Observatory. He has led multiple investigations of comets using the International Ultraviolet Explorer, the Hubble Space Telescope, and the Far Ultraviolet Spectroscopic Explorer, and he was a CoI on the Rosetta-Alice instrument. In 2005, Hal co-led the team that discovered two small satellites of Pluto (Nix and Hydra). He is a fellow of the American Astronomical Society and a full member of the International Academy of Astronautics. His email address is [hal.weaver@jhuapl.edu](mailto:hal.weaver@jhuapl.edu).



**Dennis C. Reuter**, Planetary Systems Laboratory of the Solar Systems Exploration Division, NASA Goddard Space Flight Center, Greenbelt, MD

Dennis C. Reuter is a planetary scientist and senior fellow at the Planetary Systems Laboratory of the Solar Systems Exploration Division at NASA’s Goddard Space

Flight Center. He has a BS (cum laude) in chemistry from Rensselaer Polytechnic Institute and a PhD in physical chemistry from the University of California, Berkeley. Dennis is an expert in the fields of remote sensing, radiative transfer, and spectral interpretation and has been an author on well over 100 publications. He has developed innovative spacecraft-borne remote sensing instruments based on advances in optical filter design and in focal plane detector array technology. He is the project scientist for the Ralph instrument on the New Horizons mission and the Thermal InfraRed Sensor (TIRS) on Landsat-8 and for TIRS-2 on Landsat-9, the instrument scientist/principal investigator (PI) for the OSIRIS-REx (Origins, Spectral Interpretation, Resource Identification, Security-Regolith Explorer) Visible and InfraRed Spectrometer (OVIRS) on the OSIRIS-REx sample return mission to the asteroid Benu, and the instrument PI for the L’Ralph instrument on the Lucy Mission to the Jupiter Trojans. Dennis has received numerous awards, including NASA’s Exceptional Achievement Medal in 2007, the NASA Distinguished Service Medal in 2018, and Goddard Space Flight Center’s John C. Lindsay Memorial Award for Space Science in 2020. He was a finalist for the Samuel J. Heyman Service to America Medals (Sammies) in 2016. The asteroid 4706 (1988 DR) was named 4706 Dennisreuter by the IAU in 2006. His email address is [dennis.c.reuter@nasa.gov](mailto:dennis.c.reuter@nasa.gov).



**S. Alan Stern**, Southwest Research Institute, Boulder, CO

S. Alan Stern is the associate vice president of Southwest Research Institute’s space sector. He has an MS in atmospheric sciences from the University of Texas, an MS in aerospace engineering from the University of Texas, and a PhD in astrophysics and planetary science from the University of Colorado. In 2020, NASA appointed Alan to fly to space as a researcher aboard a commercial suborbital space mission. He formerly served as NASA’s chief of space and Earth science programs. His career has taken him to numerous observatories, the South Pole, the Titanic, and the upper atmosphere aboard high-performance NASA aircraft. He has served on 29 space missions. He is a member of the US National Science Board and leads NASA’s New Horizons mission to Pluto and the Kuiper Belt as its principal investigator. He has published over 440 technical papers and

written three books. He is an associate fellow of the American Institute of Aeronautics and Astronautics (AIAA) and a fellow of the American Association for the Advancement of Science (AAAS), the Royal Astronomical Society (RAS), the American Geophysical Union (AGU), and the Explorer's Club. He was awarded the von Braun Aerospace Achievement Award, *Smithsonian Magazine's* American Ingenuity Award, American Astronautical Society's Sagan Memorial Award, and NASA's Distinguished Public Service Medal. In both 2007 and 2016, he was named to the Time 100. His email address is [astern@swri.org](mailto:astern@swri.org).



**Ivan R. Linscott**, Department of Electrical Engineering, Stanford University, Stanford, CA

Ivan R. Linscott (retired) is a physicist, radio astronomer, and planetary scientist. He retired from Stanford University and is currently on contract to the Southwest Research Institute. He has a BS in physics from Union College and a PhD in particle physics from the University of California, Berkeley. After a postdoctoral assignment at Syracuse University working at the Brookhaven National Laboratory, he joined the astronomy program at Dudley Observatory to conduct pulsar observations at the Arecibo Observatory using a state-of-the-art fast Fourier transform digital spectrometer he developed in cooperation with General Electric's Electronic Lab. Accepting an invitation and a National Research Council fellowship in 1981, he joined the NASA/Ames SETI program and the Stanford Multi-channel Spectrometer project. In 1990, he started a collaboration with Stanford's Professor Len Tyler to develop uplink radio science and onboard radio systems necessary for performing uplink occultations during spacecraft planetary encounters. He joined the New Horizons Science Team to plan and conduct radio occultation of Pluto's atmosphere radiometry of Pluto and Charon and bistatic measurements. The subsequent flyby of Arrokoth afforded additional opportunities for radio occultation, radiometry, and bistatic radar experiments.



**David J. McComas**, Princeton Plasma Physics Laboratory, Princeton University, Princeton, NJ

David J. McComas is the vice president for the Princeton Plasma Physics Laboratory (PPPL), professor of astrophysical sciences, and associated faculty in mechanical and aerospace engineering at Princeton University. He received a BS in physics from the Massachusetts Institute of Technology (MIT) and a PhD in geophysics and space physics from the University of California, Los Angeles in 1986. David is the lead co-investigator for the Solar Wind Analyzer (SWAP) for the New Horizons mission to Pluto and the principal investigator for several missions. He is a fellow of the American Physical Society (APS), American Geophysical Union (AGU), and the American Association for the Advancement of Science (AAAS) and has received numerous awards and accolades, including the National Academy of Sciences' 2023 Arctowski Medal, the European Geosciences Union's 2022 Hannes Alfvén Medal, the Scientific Committee on Solar-Terrestrial Physics (SCOSTEP) 2022 Distinguished Scientist Award, AGU's 2018 Eugene Parker Lecture, the 2014

COSPAR Space Science Award, NASA's Exceptional Public Service Medal in 2015, and AGU's James B. Macelwane Award in 1993. He has served on several boards, committees, and panels; has invented a variety of instruments and missions for space applications; and holds seven patents. David has authored over 750 scientific papers spanning topics in heliospheric, magnetospheric, solar, and planetary science as well as space instrument and mission development. His email address is [dmccomas@princeton.edu](mailto:dmccomas@princeton.edu).



**Matthew E. Hill**, Space Exploration Sector, Johns Hopkins University Applied Physics Laboratory, Laurel, MD

Matthew E. Hill is a scientist in APL's Space Exploration Sector. He has a BS in physics from Rutgers University and a PhD in physics from the University of Maryland College Park. He concentrates on experimental particle physics in the space environment, and his interests range from suprathermal pickup ions to galactic cosmic rays observed from the margins of the Sun's corona to the shallows of interstellar space. Matt has been the instrument scientist for the New Horizons PEPSSI team since the 2007 Jupiter magnetotail cruise and co-investigator (Co-I) on the mission since before the 2015 Pluto encounter. He was the 2003 recipient of the American Geophysical Union's Fred L. Scarf Award for his dissertation on anomalous cosmic ray transport phenomena, primarily studied with observations he made with the Voyager 1 and 2 Low Energy Charged Particle (LECP) instruments, an APL-led experimental investigation he later joined as Co-I and for which he was named deputy principal investigator in 2023. Additional roles on other NASA missions include deputy instrument lead and Co-I on APL's EPI-Lo instrument, the low-energy component of the Princeton-led ISOIS energetic particle suite on Parker Solar Probe, a mission built, operated, and managed at APL. He also was part of the Cassini/MIMI team. His email address is [matt.hill@jhuapl.edu](mailto:matt.hill@jhuapl.edu).



**Mihály Horányi**, Physics Department, University of Colorado Boulder, Boulder, CO

Mihály Horányi is a professor in the Physics Department at the University of Colorado Boulder. He received an MS in nuclear physics and a PhD in space physics at the Loránd Eötvös University, in Budapest, Hungary. His research interests include theoretical and experimental investigations of space and laboratory dusty plasmas. He served as a co-investigator for the dust instruments onboard the Ulysses, Galileo, and Cassini missions and as a principal investigator of the Venetia Burney Student Dust Counter (VBSDC) onboard New Horizons, the Cosmic Dust Experiment (CDE) onboard the AIM satellite, and the Lunar Dust Experiment LDEX onboard LADEE. He is the principal investigator for the Interstellar Dust Experiment (IDEX) on the upcoming IMAP mission. He is the author or coauthor of over 300 refereed publications and is a fellow of both the American Physical Society and the American Geophysical Union. Asteroid 1998 AX9 was named 164701 Horanyi by the International Astronomical Union. His email address is [Mihaly.Horanyi@lasp.colorado.edu](mailto:Mihaly.Horanyi@lasp.colorado.edu).